Atmos. Meas. Tech. Discuss., 5, 2529–2565, 2012
www.atmos-meas-tech-discuss.net/5/2529/2012/
doi:10.5194/amtd-5-2529-2012

Atmospheric Measurement Techniques Discussions

Airborne intercomparison of HO_x measurements using laser-induced fluorescence and chemical ionization mass spectrometry during ARCTAS

X. Ren[1], J. Mao[2,*], W. H. Brune[2], C. A. Cantrell[3], R. L. Mauldin III[3,], R. S. Hornbrook[3], E. Kosciuch[3], J. R. Olson[4], J. H. Crawford[4], G. Chen[4], and H. B. Singh[5]**

[1]Air Resources Laboratory, National Oceanic and Atmospheric Administration, Silver Spring, Maryland, USA
[2]Department of Meteorology, Pennsylvania State University, University Park, Pennsylvania, USA
[3]Atmospheric Chemistry Division, National Center for Atmospheric Research, Boulder, Colorado, USA
[4]Science Directorate, NASA Langley Research Center, Hampton, Virginia, USA
[5]Earth Science Division, NASA Ames Research Center, Moffett Field, California, USA
[*]now at: Geophysical Fluid Dynamics Laboratory, National Oceanic and Atmospheric Administration, Princeton, New Jersey, USA
[**]now at: University of Helsinki, Helsinki, Finland and University of Colorado, Boulder, CO, USA

Received: 2 March 2012 – Accepted: 19 March 2012 – Published: 30 March 2012

Correspondence to: X. Ren (xinrong.ren@noaa.gov)

Published by Copernicus Publications on behalf of the European Geosciences Union.

Abstract

The hydroxyl (OH) and hydroperoxyl (HO_2) radicals, collectively called HO_x, play central roles in tropospheric chemistry. Accurate measurements of OH and HO_2 are critical to examine our understanding of atmospheric chemistry. Intercomparisons of different techniques for detecting OH and HO_2 are vital to evaluate their measurement capabilities. Three instruments that measured OH and/or HO_2 radicals were deployed on the NASA DC-8 aircraft throughout Arctic Research of the Composition of the Troposphere from Aircraft and Satellites (ARCTAS), in the spring and summer of 2008. One instrument was the Penn State Airborne Tropospheric Hydrogen Oxides Sensor (ATHOS) for OH and HO_2 measurements based on Laser-Induced Fluorescence (LIF) spectroscopy. A second instrument was the NCAR Selected-Ion Chemical Ionization Mass Spectrometer (SI-CIMS) for OH measurement. A third instrument was the NCAR Peroxy Radical Chemical Ionization Mass Spectrometer (PeRCIMS) for HO_2 measurement. Formal intercomparison of LIF and CIMS was conducted for the first time on a same aircraft platform. The three instruments were calibrated by quantitative photolysis of water vapor by UV light at 184.9 nm with three different calibration systems. The absolute accuracies were ±32 % (2σ) for the LIF instrument, ±65 % (2σ) for the SI-CIMS instrument, and ±50 % (2σ) for the PeRCIMS instrument. In general, good agreement was obtained between the CIMS and LIF measurements of both OH and HO_2 measurements. Linear regression of the entire data set yields $[OH]_{CIMS} = 0.89 \times [OH]_{LIF} + 2.8 \times 10^5\,cm^{-3}$ with a correlation coefficient, $r^2 = 0.72$ for OH and $[HO_2]_{CIMS} = 0.86 \times [HO_2]_{LIF} + 3.9$ parts per trillion by volume (pptv, equivalent to pmol mol^{-1}) with a correlation coefficient, $r^2 = 0.72$ for HO_2. In general, the difference between CIMS and LIF instruments for OH and HO_2 measurements can be explained by their combined measurement uncertainties. Comparison with box model results shows some similarities for both the CIMS and LIF measurements. First, the observed-to-modeled HO_2 ratio increases greatly for higher NO mixing ratios, indicating that the model may not properly account for HO_x sources that correlate with NO.

AMTD
5, 2529–2565, 2012

Second, the observed-to-modeled OH ratio increases with increasing isoprene mixing ratios, suggesting either incomplete understanding of isoprene chemistry in the model or interferences in the measurements in environments where biogenic emissions dominate ambient volatile organic compounds.

1 Introduction

The hydroxyl radical (OH) is the primary oxidizing species in the troposphere and reacts with most natural and anthropogenic trace gases emitted into the atmosphere, thereby initiating their oxidation and final removal from the atmosphere (Logan et al., 1981; Ehhalt et al., 1991; Lelieveld et al., 2004). The hydroperoxyl radical (HO_2) is an important ozone precursor through its reaction with NO. The chemistry of OH and HO_2 (OH and HO_2 are collectively called HO_x) impacts many environmental issues such as ozone and fine particle formation. Because of the important roles OH and HO_2 play in atmospheric chemistry, it has been a high priority that OH and HO_2 are accurately measured.

Three techniques have been widely used for tropospheric OH measurements, including Laser-Induced Fluorescence (LIF, also known as FAGE – Fluorescence Assay with Gas Expansion) spectroscopy (Hard et al., 1984; Stevens et al., 1994; Holland et al., 1995; Heal et al., 1995; Kanaya et al., 2001; Dusanter et al., 2008; Martinez et al., 2010), Chemical Ionization Mass Spectrometry (CIMS) (Eisele and Tanner, 1991; Berresheim et al., 2000), and Differential Optical Laser Absorption Spectroscopy (DOAS) (Perner et al., 1976, Armerding et al., 1994; Mount et al., 1997). Over the past 15–20 yr, the sensitivity and time resolution have been significantly improved for OH measurements by LIF and CIMS, although the absolute calibrations still have relatively large uncertainties. DOAS has been used as a reference method with no calibration needed but, with a relatively long time resolution of ~100 s and detection limit of $\sim 1 \times 10^6$ molecules cm^{-3}, it has had limited use in field studies.

AMTD
5, 2529–2565, 2012

Since the mid 1990s, HO_2 has been successfully measured by LIF as OH after the conversion of HO_2 by NO (Brune et al., 1995; Mather et al., 1997). Lately, CIMS-OH instruments were adapted to measure HO_2 and organic peroxy radicals (RO_2) by amplified conversion to H_2SO_4 via OH in a chain reaction with added NO and SO_2 and using controlled ratios of NO/O_2, e.g. the RO_x Chemical Conversion/CIMS (ROXMAS) (Hanke et al., 2002) and the Peroxy Radical Chemical ionization Mass Spectrometer (PeRCIMS) (Edwards et al., 2003; Hornbrook et al., 2011).

Deployments of LIF and CIMS for OH and HO_2 measurements in ground-based field campaigns and on mobile platforms have significantly improved our understanding of HO_x chemistry and have also indicated gaps in our current knowledge. For instance, in areas strongly influenced by biogenic emissions with low NO_x mixing ratios, measured OH amounts were found to be significantly higher than modeled values (e.g. Faloona et al., 2001; Tan et al., 2001; Di Carlo et al., 2004; Ren et al., 2008; Lelieveld et al., 2008; Hofzumahaus et al., 2009; Martinez et al., 2010; Whalley et al., 2011; Lu et al., 2012). In high NO_x environments, models typically underestimate HO_2 measurements (e.g. Ren et al., 2005, 2008; Kanaya et al., 2011; Lu et al., 2012). These discrepancies imply either fundamental flaws in current understanding of tropospheric HO_x chemistry or measurement errors.

A recent study by Fuchs et al. (2011) found that previous measurements of HO_2 with LIF might be biased by interference from RO_2 radicals that are produced in the oxidation of alkenes (including isoprene) and aromatics. In another study conducted in a California forest where biogenic emissions dominate, a new chemical removal method was deployed to measure OH in parallel to the traditional FAGE method with wavelength modulation. This new method shows significantly lower OH signal compared to the traditional method (Mao et al., 2012). Because of considerable uncertainties associated with calibration and possible instrument errors, intercomparisons of different HO_x measurement techniques are thus crucial to achieve high-quality measurement data and reduce instrument uncertainties.

AMTD
5, 2529–2565, 2012

Several HO_x intercomparison studies have been conducted in the past 20 yr or so, mostly in ground-based campaigns (e.g. Eisele et al., 1994; Campbell et al., 1995; Brauers et al., 1996; Mount et al., 1997; Hofzumahaus et al., 1998; Schlosser et al., 2007). These intercomparisons of tropospheric OH measurements have been reviewed by Schlosser et al. (2009). During the HO_xComp campaign in 2005, one DOAS, one CIMS, and four LIF instruments were compared formally sampling both ambient air and the atmospheric chamber SAPHIR in Jülich, Germany. All instruments measured tropospheric OH concentrations with high sensitivity and good time resolution. Sampling inhomogeneities and calibration uncertainties could explain the discrepancies in the ambient measurements (Schlosser et al., 2009). During HO_xComp, three LIF instruments also measured HO_2 in both ambient and chamber air. Measurements from these LIF instruments were well correlated and the discrepancies were likely related to interference from water vapor and ozone in the chamber measurements and sampling inhomogeneities in the ambient measurements (Fuchs et al., 2010; Kanaya et al., 2011). In 2007, a comparison was conducted between a Matrix Isolation Electron Spin Resonance (MIESR) instrument and an LIF instrument (ROxLIF), capable of detecting HO_2 and the sum of organic peroxy radicals (RO_2), during two experiments in the SAPHIR chamber. Measurements of HO_2 agreed on average to within 5 % (Fuchs et al., 2009). In an earlier HO_2 intercomparison study, a PeRCIMS and an LIF instrument were compared for HO_2 measurement in two phases: (1) by mutual exchange of calibration sources, (2) by ambient air measurements (Ren et al., 2003). Good correlation was found in both phases. However, the LIF-measured HO_2 was higher than the CIMS measured HO_2 by a factor of 1.6 after considering a calibration change in the LIF instrument that was discovered later (Ren et al., 2008).

Airborne OH and HO_2 measurements have been compared for instruments on different aircraft flying in close-proximity or wingtip-to-wingtip (Eisele et al., 2001, 2003; Kleb et al., 2011). During the Pacific Exploratory Mission Tropics B (PEM-TB) study in 1999, LIF OH measurements on the NASA DC-8 and CIMS OH measurements on the NASA P-3B aircraft showed excellent agreement in the marine boundary layer

AMTD
5, 2529–2565, 2012

with an average measurement difference similar to the uncertainty of each technique (~ ±40 %, 2σ uncertainty). The ratio of LIF-to-CIMS OH increased from 0.8 near the surface to 1.6 at 8 km altitude (Eisele et al., 2001). During the Transport and Chemical Evolution over the Pacific (TRACE-P) campaign in 2001, excellent agreement was again obtained between the LIF and CIMS OH measurements, with a slope of 0.96 and a correlation coefficient (r^2) of 0.88, after considering the revised values for the LIF OH measurements by a factor of 1.6 higher due to a calibration error discovered later (Ren et al., 2008). The Intercontinental Chemical Transport Experiment-B (INTEX-B) campaign in 2006 involved three 40–60 min comparison periods with the Penn State LIF instrument measuring OH and HO_2 on the NASA DC-8 and two NCAR CIMS instruments measuring OH and HO_2/$HO_2 + RO_2$, respectively, on the NSF C-130. The median CIMS-HO_2 to LIF-HO_2 ratio was 1.23 with a correlation coefficient (r^2) of 0.59. The median CIMS-OH to LIF-OH ratio was 0.81, but surprisingly with very little correlation (r^2 = 0.03) (Kleb et al., 2011). Thus intercomparisons of HO_x measurements on different aircraft have been inconclusive, possibly because the instruments were not consistently sampling the same air mass or because small fluctuations in instrument performance could be occurring in the limited intercomparison periods. Deploying different HO_x instruments on one aircraft solves both of these problems and provides a more rigorous and definitive comparison.

In this study, we present a formal intercomparison of OH and HO_2 measurements performed by three different instruments aboard the NASA DC-8 aircraft during the Arctic Research of the Composition of the Troposphere from Aircraft and Satellites (ARCTAS) campaign. The three instruments were the Penn State Airborne Tropospheric Hydrogen Oxides Sensor (ATHOS) for OH and HO_2 measurements based on LIF spectroscopy, the NCAR Selected-Ion Chemical Ionization Mass Spectrometer (SI-CIMS) for OH measurement, and the NCAR Peroxy Radical Chemical Ionization Mass Spectrometer (PeRCIMS) for HO_2 measurement. These measurements were also compared to box model results to investigate similarities and differences in both CIMS and LIF measurements.

AMTD
5, 2529–2565, 2012

2 Experimental description

2.1 ARCTAS mission

The NASA ARCTAS mission was conducted in two 3-week deployments based in Alaska (April 2008, ARCTAS-A) and western Canada (June–July 2008, ARCTAS-B). Its objective was to better understand the factors driving current changes in Arctic atmospheric composition and climate. Details of the background, design, execution, and components of ARCTAS can be found in Jacob et al. (2010). The ARCTAS-B deployment was preceded by one week of flights over California sponsored by the California Air Resources Board (ARCTAS-CARB) to improve state emission inventories for greenhouse gases and aerosols and to provide observations to test and improve models of ozone and aerosol pollution. For the purpose of comparing HO_x measurement under a variety of conditions, in particular those with high NO_x and VOC levels, HO_x measurements during ARCTAS-CARB were included in the intercomparison.

2.2 LIF-HO_x instrument

OH and HO_2 radicals were measured with the Penn State ATHOS instrument. ATHOS detects OH and HO_2 with LIF spectroscopy. The technique uses a pump-down technique often called the fluorescent assay by gas expansion (FAGE) originally developed by Hard et al. (1984). A detailed description of the ATHOS instrument can be found in Faloona et al. (2004); here an abbreviated description of ATHOS is given.

Sample air is drawn into a low-pressure chamber through a pinhole inlet (1.5 mm) with a vacuum pump. The pressure of the detection chamber varies from 12 to 3 hPa from 0 to 12 km altitude, respctively. As the air passes through a laser beam, OH is excited by a spectrally narrowed laser with a pulse repetition rate of 3 kHz at one of several ro-vibronic transition lines near 308 nm ($A^2\Sigma - X^2\Pi$, $v' = 0 \leftarrow v'' = 0$). Collisional quenching of the excited state of OH is slow enough at the chamber pressure that the weak OH fluorescence extends beyond the prompt scattering (Rayleigh and wall

AMTD
5, 2529–2565, 2012

scattering) and is detected with a time-gated microchannel plate (MCP) detector. HO_2 is measured by its reaction with NO followed by LIF detection of OH. The OH and HO_2 detection axes are in series: OH is detected in the first axis and HO_2 in a second axis as reagent NO (>99 %, Matheson, Twinsburg, OH, purified through Ascarite sodium hydroxide) is added to the flow between the two axes. The OH fluorescence signal is detected 60 ns after the laser pulse has cleared in the detection cells and is recorded every 0.2 s. The laser wavelength is tuned on-resonance with an OH transition for 15 s and off-resonance for 5 s, resulting in a measurement time resolution of 20 s. The OH fluorescence signal is the difference between on-resonance and off-resonance signals.

The instrument was calibrated on the ground both in the laboratory and during the field campaign. Different sizes of pinholes were used in the calibration to produce different detection cell pressures. Monitoring laser power, Rayleigh scattering, and laser linewidth maintained this calibration in flight (Faloona et al., 2004). For the calibration, OH and HO_2 were produced through water vapor photolysis by UV light at 184.9 nm. Absolute OH and HO_2 mixing ratios were calculated by knowing the 184.9 nm photon flux, which was determined with a Cs-I phototube referenced to a NIST-calibrated photomultiplier tube, the H_2O absorption cross section, the H_2O mixing ratio, and the exposure time of the H_2O to the 184.9 nm light. The absolute uncertainty was estimated to be ±32 % for both OH and HO_2 at a 2σ confidence level. The 2σ precision for a 1-min integration time during this campaign was about 0.01 parts per trillion by volume (pptv, equivalent to pmol mol^{-1}) for OH and 0.1 pptv for HO_2. Further details about the calibration process may be found in Faloona et al. (2004).

A recent laboratory study suggests that the HO_2 measurements in some FAGE-type instruments are susceptible to interference from RO_2 species arising from the oxidation of alkenes and aromatics (Fuchs et al., 2011). A laboratory study showed that ATHOS is also affected by this interference. Compared to HO_2, the relative detection sensitivities of RO_2 are 0.68 for isoprene, 0.66 for ethene, 0.40 for cyclohexane, and 0.54 for α-pinene. Determination of sensitivities from additional alkenes and aromatics is still needed, but a mean sensitivity of 0.60 ± 0.15 is consistent with all species that

AMTD
5, 2529–2565, 2012

have been measured to date. Measured HO_2 was thus corrected by 0.6 times RO_2 (modeled) initiated from alkenes + aromatics. Due to relatively low alkene and aromatic mixing ratios during ARCTAS, this correction reflects only a decrease of HO_2 by 4 % on average.

During ARCTAS, the ATHOS nacelle inlet was mounted below a nadir plate of the forward cargo bay of the DC-8 while the lasers, electronics, and vacuum pump were housed inside the forward cargo bay (Fig. 1).

2.3 CIMS-OH instrument

The NCAR SI-CIMS instrument uses chemical conversion of ambient OH with $^{34}SO_2$ to produce $H_2^{34}SO_4$, which subsequently reacts with NO_3^- reactant ions to produce $H^{34}SO_4^-$ that is detected by a mass spectrometer. The system consists of four major sections: a shrouded inlet that straightens and slows the air flow, a chemical reaction region in which the neutral chemistry takes place, an ion reaction region in which the chemical ionization reactions occur, and a turbo molecular pumped vacuum chamber which houses a quadrupole mass spectrometer and an electron multiplier detector (Mauldin et al., 2003). The measurement technique and system used in this study have been discussed in detail elsewhere (e.g. Tanner et al., 1997; Mauldin et al., 1998, 1999).

The calibration assembly and technique have been described in Mauldin et al. (2001). Briefly, OH was produced by photolyzing a controlled amount of water vapor with a mercury lamp radiation at 184.9 nm. The amount of OH produced depended on water vapor concentration, sample flow rate, intensity of the mercury lamp, and H_2O cross section for the 184.9 nm light. During calibrations, flow rates and the ambient dew point were monitored. To determine the photon flux from the lamp at 184.9 nm, vacuum UV photo diodes mounted on an *x*/*y* traverse were used to periodically map out the light field on the ground. The quantum efficiency of these diodes was compared to a National Institute of Standards and Technologies (NIST) standard diode both prior to

AMTD
5, 2529–2565, 2012

and after the mission and were found to vary by ±12 %. Using this calibration method, the overall uncertainty of the OH concentration was ±65 % (2σ) and the detection limit in a single measurement was 2×10^5 molecules cm^{-3} (Tanner et al., 1997). For a 5-min integration, the detection limit for OH was 5×10^4 molecules cm^{-3} (Mauldin et al., 2001).

2.4 CIMS-HO_2 instrument

The NCAR PeRCIMS instrument uses a technique based on the amplified chemical conversion of ambient peroxy radicals (HO_2 and/or RO_2) into a unique ion, HSO_4^-. Peroxy radicals drawn into the inlet are converted into H_2SO_4 through the addition of NO and SO_2. H_2SO_4 is then reacted with NO_3^- to form HSO_4^- ions, which are measured by a quadrupole filter mass spectrometer and a channel electron multiplier. Measurements of the total sum of all peroxy radicals, HO_2 + RO_2 (HO_xRO_x mode) or the HO_2 component only (HO_2 mode) can be achieved through adding known concentrations of NO and SO_2 to the sample flow. When inlet [NO] and [SO_2] are low, RO_2 radicals are converted to HO_2 and can be measured as HO_xRO_x. When inlet [NO] and [SO_2] are high, the conversion efficiency of RO_2 into HO_2 is low and RO_2 radicals are converted to organic nitrites (RONO). A full description of this process and tests of conversion efficiency can be found in Edwards et al. (2003).

Recently Hornbrook et al. (2011) developed an improved method for PeRCIMS to measure HO_2 and $HO_2 + RO_2$. In this method, both [NO] and [O_2] are simultaneously varied in the chemical conversion region of the PeRCIMS inlet to change the conversion efficiency of RO_2 to HO_2 so that either primarily HO_2 or $HO_2 + RO_2$ are measured. Two modes of operation are established for ambient measurements. In the first half of the minute, RO_2 radicals are measured at close to 100 % efficiency along with HO_2 radicals (low [NO]/[O_2] = 2.5×10^{-5}) and in the second half of the minute, HO_2 is detected while the majority of ambient RO_2 radicals are measured with low efficiency, approximately 15 % (high [NO]/[O_2] = 6.8×10^{-4}). This new method was used during ARCTAS.

AMTD
5, 2529–2565, 2012

Calibration of the PeRCIMS instrument was also accomplished by the photolysis of water vapor using UV radiation (184.9 nm) from a low-pressure mercury lamp. Dry synthetic air was first humidified by passing through a saturator containing de-ionized water held at an accurately known temperature (30 °C). The humidified air was diluted with dry synthetic zero air to achieve the desired water/air ratio and the mixture with a total flow rate of about 5 standard liters per minute (SLPM) was passed into a quartz calibration cell. The PeRCIMS sampling flow rate was about 1.9 SLPM. Independent dew point instrumentation measurements of the water mixing ratio indicated that this method can produce accurate H_2O mixing ratio down to levels approaching 50 ppmv. Water was then photolyzed by the mercury lamp. The radiative output of the mercury lamp used in the calibration was determined through separate N_2O actinometry experiments (Edwards et al., 2003). Radical mixing ratios over the range of ambient levels and higher/lower values of radicals were easily generated by adjusting the lamp distance, slit width, and water vapor mixing ratio within the photolysis cell. The overall measurement uncertainty associated with this instrument was about ±50 % at a 2σ confidence level. The detection limit of PeRCIMS during this campaign was about 1.0 pptv (2σ) with 15-s integration time.

2.5 HO_x measurement comparison strategy

Frequent comparisons between instruments that measure the same atmospheric constituents are essential for producing high-quality data for complex field studies, like ARCTAS, which involve multiple investigators and multiple aircraft. These comparisons often help the investigators produce the highest quality data possible by revealing instrument operation and/or calibration issues, which the investigators can then resolve, sometimes during the field deployment.

During ARCTAS, a comparison strategy was deployed for the measurements of HO_x as well as many other species measured by different instruments. The field data comparison of these duplicate measurements was “blind”. Within 24 h after each flight, investigators, without knowledge of the other measurements, submitted their data, which

AMTD
5, 2529–2565, 2012

was directed to a restricted data depository that was accessible only by a Measurement Comparison Group (MCG). Once all of the duplicate measurements for an atmospheric constituent were in the depository, those measurements were released immediately to the ARCTAS archive. Comparisons of measurements were "blind" only for the field data phase and were not blind for the preliminary and final data submission phases. However, any changes that the investigators made during or after the field campaign had to be accompanied by an explanation of the changes. This explanation had to be submitted to the MCG as well as noted in the data submission header. To aid the post-campaign analysis of the comparisons, all duplicate measurements, from the initial field submission to final data submission, were saved along with the explanations of changes.

3 Box model description

The NASA Langley Research Center time-dependent photochemical box model was used to calculate OH, HO_2 and other reactive intermediates. The model has been described in detail in several previous studies (e.g. Crawford et al., 1999; Olson et al., 2006, 2012). The modeling approach was based on the assumption of a diurnal steady state. For a suite of simultaneous measurements of input species at a given point in time, the model integrated to find a self-consistent diurnal cycle for the computed species concentrations based on constraining selected species to the measurements. Computed concentrations at the point in time of measurement were then used as the instantaneous model results. This approach ensured that all computed species were in equilibrium with the diurnal process, which was crucial for species with lifetimes too long for simple instantaneous steady state assumptions. For input, model calculations used observations from the 1-min merged data set available on the ARCTAS public data archive (ftp://ftp-air.larc.nasa.gov/pub/ARCTAS/). The minimum set of input constraints included measurements of O_3, CO, NO, non-methane hydrocarbons (NMHC), H_2O (dew/frost point), temperature, pressure, and photolysis frequencies.

AMTD
5, 2529–2565, 2012

In addition to the required constraints described above, the model had the option to include additional constraints when measurements were available for hydrogen peroxide (H_2O_2), methyl hydrogen peroxide (CH_3OOH), nitric acid (HNO_3), and peroxy acetyl nitrate (PAN). If unavailable, these atmospheric constituents were calculated by the model based on diurnal steady state. Model calculations taking advantage of these additional constraints were referred to as "constrained". All model results discussed in this paper were taken from the standard constrained model simulations in the ARCTAS data archive and may be different from the results presented in Olson et al. (2012), where additional constraints may be included.

Sources of uncertainty in model predictions include uncertainties in kinetic and photolytic rate constants, and uncertainties in constraining observations. Estimates of total model uncertainty were obtained using Monte Carlo techniques and a sensitivity approach (Olson et al., 2012).

4 Results

4.1 Overall intercomparison

Good agreement generally was obtained between the OH and HO_2 measured by CIMS and LIF for the entire three phases of ARCTAS (Fig. 2). The linear regression exhibits $[OH]_{CIMS} = 0.89 \times [OH]_{LIF} + 2.8 \times 10^5\ cm^{-3}$ with a correlation coefficient, $r^2 = 0.72$ and $[HO_2]_{CIMS} = 0.86 \times [HO_2]_{LIF} + 3.9$ pptv with a correlation coefficient, $r^2 = 0.72$. The relatively large scatter is consistent with the large stated uncertainties. The dashed lines in Fig. 2 represent the combined measurement uncertainties: ±72 % (2σ) for $[OH]_{LIF}$ and $[OH]_{CIMS}$ and ±59 % (2σ) for $[HO_2]_{LIF}$ and $[HO_2]_{CIMS}$. An independent-samples t-test (the Student's t-test) was conducted to compare the HO_x measurements by LIF and by CIMS. Because of their low concentrations during ARCTAS-A, both OH and HO_2 concentrations were averaged into 10-min intervals for this t-test. The t-test results showed that there was no significant difference in the [OH] by LIF (mean =

AMTD
5, 2529–2565, 2012

$(2.6 \pm 2.9) \times 10^6\,cm^{-3}$) and SI-CIMS (mean = $(2.4 \pm 3.1) \times 10^6\,cm^{-3}$), with a p-value = 0.78. In a Student t-test, a p-value (significance) less than 0.05 is considered to have significant difference. No significant difference was found either in the [HO_2] by LIF (mean = 15.1 ± 12.6 pptv) and PeRCIMS (mean = 17.1 ± 12.7 pptv), with a p-value of 0.76. Both t-tests were conducted at a 95 % confidence level. These results suggest that HO_x measurements by LIF and CIMS agree generally well and the variation can be largely explained by the relatively large combined measurement uncertainties.

The overall intercomparison of CIMS and LIF HO_x measurements from each flight is outlined in Table 1. The agreement between CIMS and LIF measurements varies from flight to flight and in the three different phases. For the entire ARCTAS campaign (including ARCTAS-CARB) when both instruments were working, the mean OH concentration was $2.4 \times 10^6\,cm^{-3}$ for CIMS and $2.6 \times 10^6\,cm^{-3}$ for LIF, with a median CIMS/LIF OH ratio of 0.74. The mean HO2 mixing ratio was 17.1 pptv for CIMS and 15.1 pptv for LIF, with a median CIMS/LIF OH ratio of 1.29. Among the three phases, the best agreement was obtained during ARCTAS-CARB, with median CIMS/LIF ratios of 0.94 for OH and 1.05 for HO_2, partially because of relatively high OH and HO_2 mixing ratios during ARCTAS-CARB compared to the other two phases (Table 1). Relatively larger discrepancies exist during ARCTAS-A, with median CIMS/LIF ratios of 0.72 for OH and 1.65 for HO_2, mainly due to low levels of OH and HO_2 in the spring in Arctic. During ARCTAS-A, the mean and median OH levels in each flight (except the transit flights from and to Palmdale, California) were below $1 \times 10^6\,cm^{-3}$ and OH concentrations were often lower than or around the detection limits of both instruments. HO_2 mixing ratios were also low during ARCTAS-A, with mean and median levels varying from 2 to 6 pptv if the transit flights from and to Palmdale, California are excluded.

4.2 Comparison as a function of altitude

Comparison of OH measurements by CIMS and LIF as a function of altitude shows that at altitudes below 4–5 km, the median CIMS/LIF OH ratios are close to one, but

AMTD
5, 2529–2565, 2012

the ratios fall well below 1 above 5 km in all three phases (Fig. 3). These results are very similar to the comparison results from the two previous studies: PEM-TB and TRACE-P (Eisele et al., 2001, 2003). During PEM-TB, which was conducted in the tropical Pacific, two brief intercomparisons in close proximity were conducted between the LIF instrument on the NASA DC-8 and the CIMS OH instrument on the NASA P3-B. Excellent agreement was obtained between two aircraft OH measurements in the marine boundary layer, but the CIMS/LIF OH ratio was only about 0.6 at the 5.5 km flight leg. Lower CIMS/LIF OH ratios at higher altitudes were also observed from 25° N latitude to 25° S latitude (Eisele et al., 2001). A similar increasing trend in CIMS/LIF OH ratio at higher altitudes was also observed in three side-by-side flights between the NASA DC-8 and the P-3B during TRACE-P, which was conducted off the coast of Asia with air often quite polluted (Eisele et al., 2003).

The altitude dependence of the CIMS/LIF HO_2 ratio is quite different from that of the OH ratio. During ARCTAS-A, the CIMS HO_2 were consistently higher than the LIF HO_2 by a factor of 1.72 ± 0.28 from the surface to 10 km with little altitude dependence on average (Fig. 4a). This difference is significant considering the combined uncertainty (±59 %) of the CIMS and LIF HO_2 measurements. For median ratios in 1-km altitude bins, a Student's t-test also shows this significant difference between the HO_2 measurements by LIF (mean = 3.8 ± 2.6 pptv) and CIMS (mean = 6.3 ± 4.2 pptv) with a p-value of only 0.02 at a 95 % conference level. However, during both ARCTAS-CARB and ARCTAS-B, the CIMS/LIF HO_2 ratios are close to 1 below 6 km and Student's t-tests show no significant difference between the two measurements with p-values of 0.77 for ARCTAS-CARB and 0.15 for ARCAS-B. Above 6 km, the ratio increases from 1 to 2 (Fig. 4b and c) and the difference is significant.

4.3 Comparison with box model

Although this study focuses on the measurement intercomparisons, a comparison with the model results can provide some insight into the measurement differences. In addition, it can indicate potential problems with chemical mechanisms when measurements

AMTD
5, 2529–2565, 2012

from the instruments agree but disagree with the model results. The model simulations with additional constraints including H_2O_2, CH_3OOH, HNO_3, and PAN were used in this comparison.

In general the LIF-OH agrees well with the modeled OH during ARCTAS-A and ARCTAS-CARB, with little altitude dependence. However, the LIF OH is generally greater than the modeled OH below 8 km during ARCTAS-B, with a median LIF/model OH ratio of 1.3 (Fig. 5). For mean ratios in 1-km altitude bins, Student's t-tests show no significant difference between the measured OH by LIF and the modeled OH with a p-value of 0.42 for ARCTAS-A, 0.66 for ARCTAS-CARB, and 0.47 for ARCTAS-B at a 95 % conference level.

The CIMS OH agrees well with the modeled OH below 6 km, but falls well below the modeled OH above 6 km during the ARCTAS-A and ARCTAS-CARB phases. During ARCTAS-B, the CIMS OH is in good agreement with the modeled OH between 2–4 km, but the CIMS/model OH ratio is generally greater than 1 below 2 km but less than 1 above 5 km (Fig. 5). Student's t-tests show no significant difference between the CIMS OH and modeled OH for the entire ARCTAS-B (p-value = 0.68) and below 6 km during ARCTAS-A (p-value = 0.52) and ARCTAS-CARB (p-value = 0.91) but show significant difference above 6 km during ARCTAS-A (p-value = 0.006) and ARCTAS-CARB (p-value = 0.001).

For HO_2, both CIMS and LIF measurements agree with the model below 6 km during ARCTAS-CARB and ARCTAS-B, but the LIF HO_2 is slightly lower, and the CIMS HO_2 is slightly greater, than the model predictions above 6 km (Fig. 6). During ARCTAS-A, the CIMS HO_2 agrees well with the modeled HO_2 between 2 km and 9 km, although the CIMS HO_2 is slightly greater than the modeled HO_2 for altitudes below 2 km or above 9 km. The median LIF/model HO_2 ratio is 0.79 during ARCTAS-A. For mean ratios in 1-km altitude bins, Student's t-tests show significant difference between the LIF HO_2 and modeled HO_2 during ARCTAS-A (p-value = 0.008), but no significant difference during ARCTAS-CARB (p-value = 0.72) and ARCTAS-B (p-value = 0.07). The t-tests also show significant difference between the CIMS HO_2 and modeled HO_2

AMTD
5, 2529–2565, 2012

during ARCTAS-CARB (p-value = 0.04), but no significant difference during ARCTAS-A (p-value = 0.68) and ARCTAS-B (p-value = 0.48). In fact, an HO_2 uptake by aerosols has been proposed to explain this model overestimate of LIF HO_2 during ARCTAS-A (Mao et al., 2010). This HO_2 uptake was expected to have less impact on HO_2 concentrations during ARCTAS-CARB and ARTCAS-B because of the relatively fast gas-phase photochemistry during these two phases.

4.4 Comparison as a function of NO

Nitric oxide (NO) plays a key role in HO_x photochemistry by cycling HO_2 to OH, so it is important to conduct observation-to-model comparisons as a function of NO. The observed-to-modeled HO_2 ratio increases for higher NO levels, as seen by both LIF and CIMS (Fig. 7, middle). This hints that there are missing HOx sources in the model that correlate with NO. It is worthwhile to note that during ARCTAS 90 % of the NO mixing ratios were less than 100 pptv, so there are limited data points at higher NO (e.g. NO > 1 parts per billion by volume (ppbv, equivalent to nmol mol^{-1})). When the model was constrained to the measured H_2O_2 and HCHO, the measured-to-modeled HO_2 ratio is 0.69 for NO < 100 pptv and 1.2 for NO>100 pptv. The trend of the higher-than-predicted HO_2 at high NO remains with this additional constraints (Olson et al., 2012). The modeled OH is lower than the LIF-OH at low NO levels but lower than the CIMS-OH at high NO levels, indicating that there is difference between LIF and CIMS measurements at low and high NO mixing ratios. When the NO levels are between ~10 pptv and ~1 ppbv, the observed-to-modeled OH ratios are close to 1 for both LIF and CIMS. Because of the higher CIMS-OH than the modeled OH at high NO levels, the observed-modeled HO_2/OH ratios for CIMS are close to 1 despite the higher-than-expected HO_2 at high NO levels (Fig. 7, bottom). For LIF, the observed-to-modeled HO_2/OH ratio increases as NO level increases, consistent with the gradual increasing of the observed-to-modeled HO_2 ratio as NO increases.

AMTD
5, 2529–2565, 2012

4.5 Comparison as a function of isoprene

Similar to the Intercontinental Chemical Transport Experiment-A (INTEX-A) in 2004 and the Program for Research on Oxidants: PHotochemistry, Emissions and Transport in summer 1998 (PROPHET 1998) (Ren et al., 2008), the observed-to-modeled OH ratio is frequently much greater than 1.0 below 2 km altitude at high isoprene levels during ARCTAS-CARB and ARCTAS-B (Fig. 8). More interestingly, very similar isoprene dependence of observed-to-modeled OH ratio was observed for both CIMS and LIF, two fundamentally different techniques. The observed-to-modeled OH ratio increases slowly from 1.0 to 2 as isoprene increases from less than 20 pptv to 500 pptv, but for isoprene levels exceeding 500 pptv, the observed-to-modeled OH ratio rapidly increases to ~6 as isoprene increases to 6–8 ppbv. In contrast, the observed-to-modeled HO_2 ratios have little dependence on isoprene for both CIMS and LIF (Fig. 8).

The reasons for the higher-than-expected measured OH at high isoprene levels are not clear, but much of the discrepancy for the ATHOS LIF OH can be explained by an unknown measured interference. The OH concentrations measured by LIF are likely higher than the actual values in environments when biogenic emissions dominate (Mao et al., 2012). A new chemical removal method using hexafluoropropylene (C_3F_6) to measure OH was deployed in parallel with the traditional FAGE method during BEARPEX 2009, a field intensive study ina California forest east of Sacramento. The new method gives on average only 40–50 % of the OH from the traditional method. The discrepancy was found to be temperature-dependent, with lower influence under lower temperatures. The interference is possibly due to internally generated OH, possibly from oxidation of biogenic volatile organic compounds. Unfortunately this new chemical removal method was not used for the LIF OH measurements during ARCTAS, so the level of this interference could not be quantified. It is unclear why the measured-to-modeled OH ratios for CIMS and LIF agree so well as a function of isoprene during ARCTAS, since OH measured by CIMS has typically been less than OH measured by LIF in forests (Schlosser et al., 2009). Both LIF and CIMS instruments need to be

AMTD
5, 2529–2565, 2012

further tested in the laboratory regarding potential instrument artifacts in environments where biogenic emissions dominate.

At the same time, the amount of OH production from isoprene oxidation is still being debated. A few recent studies have suggested regeneration of OH in the photooxidation of isoprene either through the formation of epoxides (Paulot et al., 2009) or isomerization of isoprene peroxy radicals (Peeters et al., 2009; Peeters and Müller, 2010). These mechanisms of OH regeneration in isoprene oxidation have not been included in the current box model simulations for ARCTAS. Including these mechanisms in the model might shed light on some of the discrepancy.

5 Summary

A formal intercomparison of OH and HO_2 measured with two fundamentally different techniques, LIF and CIMS, was conducted successfully for the first time on the same aircraft platform during ARCTAS. Good agreement in general was observed. Linear regression results show that $[OH]_{CIMS} = 0.89 \times [OH]_{LIF} + 2.8 \times 10^5\ cm^{-3}$ with a correlation coefficient, $r^2 = 0.72$ for OH and $[HO_2]_{CIMS} = 0.86 \times [HO_2]_{LIF} + 3.9$ pptv with a correlation coefficient, $r^2 = 0.72$ for HO_2. The difference between the CIMS and LIF instruments for OH and HO_2 measurements can be generally explained by their combined measurement uncertainties.

Comparison with box model results shows some similarities for both CIMS and LIF measurements. First, the observed and modeled HO_2 ratio increases greatly for higher NO levels, indicating that the model may miss HO_x sources that correlate with elevated NO. Second, the observed-to-modeled OH ratio in the planetary boundary layer in forested regions is a strong function of isoprene. It increases slowly from 1.0 to 2.0 as isoprene increases from ~20 pptv to 500 pptv, but for isoprene levels exceeding 500 pptv, the observed-to-modeled OH ratio rapidly increased to ~6. This isoprene dependence of observed-to-modeled OH ratio is consistent with the results in INTEX-A and PROPHET 1998, indicating either incomplete understanding of isoprene chemistry

AMTD
5, 2529–2565, 2012

in the model or an interference in the measurements in environments where biogenic emissions dominate ambient volatile organic compounds.

Acknowledgements. This work was supported by the NASA Tropospheric Chemistry Program (NNH07ZDA001N-ARCTAS and NNX08AH67G). The authors thank the DC-8 management, crew, and support staff during the ARCTAS preparation and deployment for making the field study successful. The authors also thank other ARCTAS research groups for the use of their data in the model.

References

Armerding, W., Spiekermann, M., and Comes, F. J.: OH multipass absorption: Absolute and in situ method for local monitoring of tropospheric hydroxyl radicals, J. Geophys. Res., 99, 1225–1239, 1994.

Berresheim, H., Elste, T., Plass-Dülmer, C., Eisele, F. L., and Tanner, D. J.: Chemical ionization mass spectrometer for long-term measurements of atmospheric OH and H_2SO_4, Int. J. Mass Spectrom., 202, 91–109, 2000.

Brauers, T., Aschmutat, U., Brandenburger, U., Dorn, H.-P., Hausmann, M., Heβling, M., Hofzumahaus, A., Holland, F., Plass-Dulmer, C., and Ehhalt, D. H.: Intercomparison of tropospheric OH radical measurements by multiple folded long-path laser absorption and laser induced fluorescence, Geophys. Res. Lett., 23, 2545–2548, 1996.

Brune, W. H., Stevens, P. S., and Mather, J. H.: Measuring OH and HO_2 in the troposphere by laser-induced fluorescence at low pressure, J. Atmos. Sci., 52, 3328–3336, 1995.

Campbell, M. J., Hall, B. D., Sheppard, J. C., Utley, P. L., O'Brien, R. J., Hard, T. M., and George, L. A.: Intercomparison of local hydroxyl measurements by radiocarbon and FAGE techniques, J. Atmos. Sci., 52, 3421–3427, 1995.

Carslaw, N., Jacobs, P. J., and Pilling, M. J.: Modeling OH, HO_2, and RO_2 radicals in the marine boundary layer: 2. Mechanism reduction and uncertainty analysis, J. Geophys. Res., 104, 30257–30273, 1999.

Crawford, J., Davis, D., Olson, J., Chen, G., Liu, S., Gregory, G., Barrick, J., Sachse, G., Sandholm, S., Heikes, B., Singh, H., and Blake, D.: Assessment of upper tropospheric HOx source over the tropical Pacific based on NASA GTE/PEM data: Net affect on HO_x and other photochemical parameters, J. Geophys. Res., 104, 16255–16273, 1999.

AMTD

5, 2529–2565, 2012

Creasey, D. J., Halford-Maw, P. A., Heard, D. E., Pilling, M. J., and Whitaker, B. J.: Implementation and initial deployment of a field instrument for measurement of OH and HO_2 in the troposphere by laser-induced fluorescence, J. Chem. Soc. Faraday Trans., 16, 2907–2913, 1997.

Di Carlo, P., Brune, W. H., Martinez, M., Harder, H., Lesher, R., Ren, X., Thornberry, T., Carroll, M. A., Young, V., Shepson, P. B., Riemer, D., Apel, E., and Campbell, C.: Missing OH reactivity in a forest: Evidence for unknown reactive biogenic VOCs, Science 304, 722–725, 2004.

Dusanter, S., Vimal, D., and Stevens, P. S.: Technical note: Measuring tropospheric OH and HO_2 by laser-induced fluorescence at low pressure. A comparison of calibration techniques, Atmos. Chem. Phys., 8, 321–340, doi:10.5194/acp-8-321-2008, 2008.

Edwards, G. D., Cantrell, C. A., Stephens, S., Hill, B., Goyea, O., Shetter, R. E., Mauldin, R. L., Kosciuch, E., Tanner D. J., and Eisele, F. L.: Chemical Ionization Mass Spectrometer instrument for the measurement of tropospheric HO_2 and RO_2, Anal. Chem., 75, 5317–5327, 2003.

Ehhalt, D. H., Dorn, H.-P., and Poppe, D.: The chemistry of the hydroxyl radical in troposphere, Proc. Royal. Soc. Ed. 97B, 17–34, 1991.

Eisele, F. L. and Tanner, D. J.: Ion-assisted tropospheric OH measurements, J. Geophys. Res., 96, 9295–9308, 1991.

Eisele, F. L., Mount, G. H., Fehsenfeld, F. C., Harder, J., Marovich, E., Parrish, D. D., Roberts, J., Trainer, M., and Tanner, D.: Intercomparison of tropospheric OH and ancillary trace gas measurements at Fritz Peak Observatory, Colorado, J. Geophys. Res., 99, 18605–18626, 1994.

Eisele, F. L., Mauldin, R. L., Ranner, D. J., Cantrell, C., Kosciuch, E., Nowak, J. B., Brune, B., Faloona, I., Tan, D., Davis, D. D., Wang, L., and Chen, G.: Relationship between OH measurements on two different NASA aircraft during PEM Tropics B, J. Geophys. Res., 106, 32683–32689, 2001.

Eisele, F. L., Mauldin, L., Cantrell, C., Zondlo, M., Apel, E., Fried, A., Walega, J., Shetter, R., Lefer, B., Flocke, F., Weinheimer, A., Avery, M., Vay, S., Sachse, G., Podolske, J., Diskin, G., Barrick, J. D., Singh, H. B., Brune, W., Harder, H., Martinez, M., Bandy, A., Thornton, D., Heikes, B., Kondo, Y., Riemer, D., Sandholm, S., Tan, D., Talbot, R., and Dibb, J.: Summary of measurement intercomparisons during TRACE-P, J. Geophys. Res., 108, 8791, doi:10.1029/2002JD003167, 2003.

AMTD
5, 2529–2565, 2012

Faloona, I., Tan, D., Brune, W., Hurst, J., Barket Jr., D., Couch, T. L., Shepson, P., Apel, E., Riemer, D., Thornberry, T., Carroll, M. A., Sillman, S., Keeler, G. J., Sagady, J., Hooper, D., and Paterson, K., Nighttime observations of anomalously high levels of hydroxyl radicals above a deciduous forest canopy, J. Geophys. Res., 106, 24315–24333, 2001.

Faloona, I. C., Tan, D., Lesher, R. L., Hazen, N. L., Frame, C. L., Simpas, J. B., Harder, H., Martinez, M., Di Carlo, P., Ren, X., and Brune, W. H.: A laser-induced fluorescence instrument for detecting tropospheric OH and HO_2: Characteristics and calibration, J. Atmos. Chem., 47, 139–167, 2004.

Fuchs, H., Brauers, T., Häseler, R., Holland, F., Mihelcic, D., Müsgen, P., Rohrer, F., Wegener, R., and Hofzumahaus, A.: Intercomparison of peroxy radical measurements obtained at atmospheric conditions by laser-induced fluorescence and electron spin resonance spectroscopy, Atmos. Meas. Tech., 2, 55–64, doi:10.5194/amt-2-55-2009, 2009.

Fuchs, H., Brauers, T., Dorn, H.-P., Harder, H., Häseler, R., Hofzumahaus, A., Holland, F., Kanaya, Y., Kajii, Y., Kubistin, D., Lou, S., Martinez, M., Miyamoto, K., Nishida, S., Rudolf, M., Schlosser, E., Wahner, A., Yoshino, A., and Schurath, U.: Technical Note: Formal blind intercomparison of HO_2 measurements in the atmosphere simulation chamber SAPHIR during the HOxComp campaign, Atmos. Chem. Phys., 10, 12233–12250, doi:10.5194/acp-10-12233-2010, 2010.

Fuchs, H., Bohn, B., Hofzumahaus, A., Holland, F., Lu, K. D., Nehr, S., Rohrer, F., and Wahner, A.: Detection of HO_2 by laser-induced fluorescence: calibration and interferences from RO_2 radicals, Atmos. Meas. Tech., 4, 1209–1225, doi:10.5194/amt-4-1209-2011, 2011.

Hanke, M., Uecker, J., Reiner, T., and Arnold, F.: Atmospheric peroxy radicals: ROXMAS, a new mass-spectrometric methodology for speciated measurements of HO_2 and RO_2 and first results, Int. J. Mass Spectrom., 213, 91–99, 2002.

Hard, T. M., O'Brian, R. J., Chan, C. Y., and Mehrabzadeh, A. A.: Tropospheric free radical determination by FAGE, Environ. Sci. Technol., 18, 768–777, 1984.

Hasson, A. S., Tyndall, G. S., and Orlando, J. J.: A product yield study of the reaction of HO_2 radicals with ethyl peroxy ($C_2H_5O_2$), acetyl peroxy ($CH_3C(O)O_2$), and acetonyl peroxy ($CH_3C(O)CH_2O_2$) radicals, J. Phys. Chem. A, 108, 5979–5989, 2004.

Heal, M. R., Heard, D. E., Pilling, M. J., and Whitker, B. J.: On the development and validation of FAGE for local measurement of tropospheric OH and HO_2, J. Atmos. Sci., 52, 3428–3441, 1995.

AMTD
5, 2529–2565, 2012

Hofzumahaus, A., Aschmutat, U., Brandenburger, U., Brauers, T., Dorn, H.-P., Hausmann, M., Hessling, M., Holland, F., and Plass-Dülmer, C.: Intercomparison of tropospheric OH measurements by different laser techniques during the POPCORN campaign 1994, J. Atmos. Chem., 31, 227–246, 1998.

Hofzumahaus, A., Rohrer, F., Lu, K., Bohn, B., Brauers, T., Chang, C.-C., Fuchs, H., Holland, F., Kita, K., Kondo, Y., Li, X., Lou, S., Shao, M., Zeng, L., Wahner, A., and Zhang, Y.: Amplified trace gas removal in the troposphere, Science, 324, 1702–1704, doi:10.1126/science.1164566, 2009.

Holland, F., Hessling, M., and Hofzumahaus, A.: In situ measurement of tropospheric OH radicals by laser-induced fluorescence – a description of the KFA instrument, J. Atmos. Sci., 52, 3393–3401, 1995.

Hornbrook, R. S., Crawford, J. H., Edwards, G. D., Goyea, O., Mauldin III, R. L., Olson, J. S., and Cantrell, C. A.: Measurements of tropospheric HO_2 and RO_2 by oxygen dilution modulation and chemical ionization mass spectrometry, Atmos. Meas. Tech., 4, 735–756, doi:10.5194/amt-4-735-2011, 2011.

Jacob, D. J., Crawford, J. H., Maring, H., Clarke, A. D., Dibb, J. E., Emmons, L. K., Ferrare, R. A., Hostetler, C. A., Russell, P. B., Singh, H. B., Thompson, A. M., Shaw, G. E., McCauley, E., Pederson, J. R., and Fisher, J. A.: The Arctic Research of the Composition of the Troposphere from Aircraft and Satellites (ARCTAS) mission: design, execution, and first results, Atmos. Chem. Phys., 10, 5191–5212, doi:10.5194/acp-10-5191-2010, 2010.

Kanaya, Y., Sadanaga, Y., Hirokawa, Kajii, Y., and Akimoto, H.: Development of a ground-based LIF instrument for measuring HO_x radicals: Instrumentation and calibrations, J. Atmos. Chem., 38, 73–110, 2001.

Kanaya, Y., Hofzumahaus, A., Dorn, H.-P., Brauers, T., Fuchs, H., Holland, F., Rohrer, F., Bohn, B., Tillmann, R., Wegener, R., Wahner, A., Kajii, Y., Miyamoto, K., Nishida, S., Watanabe, K., Yoshino, A., Kubistin, D., Martinez, M., Rudolf, M., Harder, H., Berresheim, H., Elste, T., Plass-Dülmer, C., Stange, G., Kleffmann, J., Elshorbany, Y., and Schurath, U.: Comparisons of observed and modeled OH and HO_2 concentrations during the ambient measurement period of the HOxComp field campaign, Atmos. Chem. Phys., 12, 2567–2585, doi:10.5194/acp-12-2567-2012, 2012.

Kleb, M. M., Chen, G., Crawford, J. H., Flocke, F. M., and Brown, C. C.: An overview of measurement comparisons from the INTEX-B/MILAGRO airborne field campaign, Atmos. Meas. Tech., 4, 9–27, doi:10.5194/amt-4-9-2011, 2011.

AMTD
5, 2529–2565, 2012

Kwan, A. J., Chan, A. W. H., Ng, N. L., Kjaergaard, H. G., Seinfeld, J. H., and Wennberg, P. O.: Peroxy radical chemistry and OH radical production during the NO_3-initiated oxidation of isoprene, Atmos. Chem. Phys. Discuss., 12, 2259–2302, doi:10.5194/acpd-12-2259-2012, 2012.

Lelieveld, J., Dentener, F. J., Peters, W., and Krol, M. C.: On the role of hydroxyl radicals in the self-cleansing capacity of the troposphere, Atmos. Chem. Phys., 4, 2337–2344, doi:10.5194/acp-4-2337-2004, 2004.

Lelieveld, J., Butler, T. M., Crowley, J., Dillon, T., Fischer, H., Ganzeveld, L., Harder, H., Lawrence, M. G., Martinez, M., Taraborrelli, D., and Williams, J.: Atmospheric oxidation capacity sustained by a tropical forest, Nature, 452, 737–740, 2008.

Logan, J. A., Prather, M. J., Wofsy, S. C., and McElroy, M. B.: Tropospheric chemistry: A global perspective, J. Geophys. Res., 86, 7210–7254, 1981.

Lu, K. D., Rohrer, F., Holland, F., Fuchs, H., Bohn, B., Brauers, T., Chang, C. C., Häseler, R., Hu, M., Kita, K., Kondo, Y., Li, X., Lou, S. R., Nehr, S., Shao, M., Zeng, L. M., Wahner, A., Zhang, Y. H., and Hofzumahaus, A.: Observation and modelling of OH and HO_2 concentrations in the Pearl River Delta 2006: a missing OH source in a VOC rich atmosphere, Atmos. Chem. Phys., 12, 1541–1569, doi:10.5194/acp-12-1541-2012, 2012.

Mao, J., Jacob, D. J., Evans, M. J., Olson, J. R., Ren, X., Brune, W. H., Clair, J. M. St., Crounse, J. D., Spencer, K. M., Beaver, M. R., Wennberg, P. O., Cubison, M. J., Jimenez, J. L., Fried, A., Weibring, P., Walega, J. G., Hall, S. R., Weinheimer, A. J., Cohen, R. C., Chen, G., Crawford, J. H., McNaughton, C., Clarke, A. D., Jaeglé, L., Fisher, J. A., Yantosca, R. M., Le Sager, P., and Carouge, C.: Chemistry of hydrogen oxide radicals (HO_x) in the Arctic troposphere in spring, Atmos. Chem. Phys., 10, 5823–5838, doi:10.5194/acp-10-5823-2010, 2010.

Mao, J., Ren, X., Brune, W. H., Van Duin, D. M., Cohen, R. C., Park, J.-H., Goldstein, A. H., Paulot, F., Beaver, M. R., Crounse, J. D., Wennberg, P. O., DiGangi, J. P., Henry, S. B., Keutsch, F. N., Park, C., Schade, G. W., Wolfe, G. M., and Thornton, J. A.: Insights into hydroxyl measurements and atmospheric oxidation in a California forest, Atmos. Chem. Phys. Discuss., 12, 6715–6744, doi:10.5194/acpd-12-6715-2012, 2012.

Martinez, M., Harder, H., Kubistin, D., Rudolf, M., Bozem, H., Eerdekens, G., Fischer, H., Klüpfel, T., Gurk, C., Königstedt, R., Parchatka, U., Schiller, C. L., Stickler, A., Williams, J., and Lelieveld, J.: Hydroxyl radicals in the tropical troposphere over the Suriname rainforest: airborne measurements, Atmos. Chem. Phys., 10, 3759–3773, doi:10.5194/acp-10-3759-2010, 2010.

AMTD
5, 2529–2565, 2012

Mather, J. H., Stevens, P. S., and Brune, W. H.: OH and HO_2 measurements using laser-induced fluorescence, J. Geophys. Res., 102, 6427–6436, 1997.
Mauldin III, R. L., Tanner, D. J., Frost, G. J., Chen, G., Prevot, A. S. H., Davis, D. D., and Eisele, F. L.: OH measurements during ACE-1: observations and model comparisons, J. Geophys. Res., 103, 16713–16729, 1998.
Mauldin III, R. L., Tanner, D. J., Frost, G. J., Chen, G., Prevot, A. S. H., Davis, D. D., and Eisele, F. L.: OH measurements during PEM-Tropics A, J. Geophys. Res., 104, 5817–5827, 1999.
Mauldin III, R. L., Eisele, F. L., Cantrell, C. A., Kosciuch, E., Ridley, B. A., Lefer, B., Tanner, D. J., Nowak, J. B., Chen, G., Wang, L., and Davis, D.: Measurements of OH aboard the NASA P-3 during PEM-Tropics B, J. Geophys. Res., 106, 32657– 32666, 2001.
Mauldin III, R. L., Cantrell, C. A., Zondlo, M., Kosciuch, E., Eisele, F. L., Chen,, G., Davis, D., Weber, R., Crawford, J., Blake, D., Bandy, A., and Thornton, D.: Highlights of OH, H_2SO_4, and methane sulfonic acid measurements made aboard the NASA P-3B during Transport and Chemical Evolution over the Pacific, J. Geophys. Res., 108, 8796, doi:10.1029/2003JD003410, 2003.
Mount, G. H., Eisele, F. L., Tanner, D. J., Brault, J. W., Johnston, P. V., Harder, J. W., Williams, E. J., Fried, A., and Shetter, R.: An intercomparison of spectroscopic laser long-path and ion-assisted in situ measurements of hydroxyl concentrations during the Tropospheric OH Photochemistry Experiment, fall 1993, J. Geophys. Res., 102, 6437–6455, 1997.
Olson, J. R., Crawford, J. H., Chen, G., Brune, W. H., Faloona, I. C., Tan, D., Harder, H., and Martinez, M.: A reevaluation of airborne HO_x observations from NASA field campaigns, J. Geophys Res., 111, D10301, doi:10.1029/2005JD006617, 2006.
Olson, J. R., Crawford, J. H., Chen, G., Brune, W. H., Mao, J., Ren, X., Fried, A., Weibring, P., Walega, J., Weinheimer, A., Knapp, D., Apel, E., Hall S., Wennberg, P., Crounse, J., and St. Clair, J.: An analysis of fast photochemistry over high northern latitudes during spring and summer using in-situ observations from ARCTAS and TOPSE, Atmos. Chem. Phys., submitted, 2012.
Paulot, F., Crounse, J. D., Kjaergaard, H. G., Kürten, A., St. Clair, J. M., Seinfeld, J. H., and Wennberg, P. O.: Unexpected epoxide formation in the gas-phase photooxidation of isoprene, Science, 325, 730–733, doi:10.1126/science.1172910, 2009.
Peeters, J., Nguyen, T. L., and Vereecken, L.: HO_x radical regeneration in the oxidation ofisoprene, Phys. Chem. Chem. Phys., 11, 5935–5939, 2009.

AMTD
5, 2529–2565, 2012

Peeters, J. and Müller, J.-F.: HO_x radical regeneration in isoprene oxidation via peroxy radical isomerisations, II: Experimental evidence and global impact, Phys. Chem. Chem. Phys., 12, 14227–14235, 2010.

Perner, D., Ehhalt, D. H., Pätz, H.-W., Platt, U., Röth, E. P., and Volz, A.: OH radicals in the lower troposphere, Geophys. Res. Lett., 3, 466–468, 1976.

Ren, X., Edwards, G. D., Cantrell, C. A., Lesher, R. L., Metcalf, A. R., Shirley, T., and Brune W. H.: Intercomparison of peroxy radical measurements at a rural site using laser-induced fluorescence and Peroxy Radical Chemical Ionization Mass Spectrometer (PeRCIMS) techniques, J. Geophys. Res., 108, 4605, doi:10.1029/2003JD003644, 2003.

Ren, X., Brune, W. H., Cantrell, C. A., Edwards, G. D., Shirley, T., Metcalf, A. R., and Lesher, R. L.: Hydroxyl and peroxy radical chemistry in a rural area of Central Pennsylvania: Observations and model comparisons, J. Atmos. Chem., 52, 231–257, 2005.

Ren, X., Olson, J. R., Crawford, J. H., Brune, W. H., Mao, J., Long, R. B., Chen, Z., Chen, G., Avery, M. A., Sachse, G. W., Barrick, J. D., Diskin, G. S., Huey, L. G., Fried, A., Cohen, R. C., Heikes, B., Wennberg, P. O., Singh, H. B., Blake, D. R., and Shetter, R. E.: HO_x chemistry during INTEX-A 2004: Observation, model calculation, and comparison with previous studies, J. Geophys. Res., 113, D05310, doi:10.1029/2007JD009166, 2008.

Schlosser, E., Bohn, B., Brauers, T., Dorn, H.-P., Fuchs, H., Häseler, R., Hofzumahaus, A., Holland, F., Rohrer, F., Rupp, L. O., Siese, M., Tillmann, R., and Wahner, A.: Intercomparison of two hydroxyl radical measurement techniques at the atmosphere simulation chamber SAPHIR, J. Atmos. Chem., 56, 187–205, 2007.

Schlosser, E., Brauers, T., Dorn, H.-P., Fuchs, H., Häseler, R., Hofzumahaus, A., Holland, F., Wahner, A., Kanaya, Y., Kajii, Y., Miyamoto, K., Nishida, S., Watanabe, K., Yoshino, A., Kubistin, D., Martinez, M., Rudolf, M., Harder, H., Berresheim, H., Elste, T., Plass-Dülmer, C., Stange, G., and Schurath, U.: Technical Note: Formal blind intercomparison of OH measurements: results from the international campaign HO_xComp, Atmos. Chem. Phys., 9, 7923–7948, doi:10.5194/acp-9-7923-2009, 2009.

Stevens, P. S., Mather, J. H., and Brune, W. H.: Measurement of tropospheric OH and HO_2 by laser-induced fluorescence at low pressure, J. Geophys. Res., 99, 3543–3557, 1994.

Tan, D., Faloona, I., Simpas, J. B., Brune, W., Shepson, P. B., Couch, T. L., Sumner, A. L., Carroll, M. A., Thornberry, T., Apel, E., Riemer, D., and Stockwell, W.: HO_x budgets in a deciduous forest: Results from the PROPHET summer 1998 campaign, J. Geophys. Res., 106, 24407–24427, 2001.

AMTD
5, 2529–2565, 2012

Tanner, D., Jefferson, A., and Eisele, F.: Selected ion chemical ionization mass spectrometric measurement of OH, J. Geophys. Res., 102, 6415–6425, 1997.

Thompson, A. M. and Stewart, R. W.: Effect of chemical kinetics uncertainties on calculated constituents in a tropospheric photochemical model, J. Geophys. Res., 96, 13089–13108, 1991.

Whalley, L. K., Edwards, P. M., Furneaux, K. L., Goddard, A., Ingham, T., Evans, M. J., Stone, D., Hopkins, J. R., Jones, C. E., Karunaharan, A., Lee, J. D., Lewis, A. C., Monks, P. S., Moller, S. J., and Heard, D. E.: Quantifying the magnitude of a missing hydroxyl radical source in a tropical rainforest, Atmos. Chem. Phys., 11, 7223–7233, doi:10.5194/acp-11-7223-2011, 2011.

AMTD

5, 2529–2565, 2012

Table 1. Overall comparison of OH and HO_2 measured with LIF and CIMS during ARCTAS.

Flt #	Flight Description	$[OH]_{CIMS}$ (cm^{-3})		$[OH]_{LIF}$ (cm^{-3})		$[OH]_{CIMS}/[OH]_{LIF}$		$[HO_2]_{CIMS}$ (pptv)		$[HO_2]_{LIF}$ (pptv)		$[HO_2]_{CIMS}/[HO_2]_{LIF}$	
		mean	median	Mean	median	mean	median	mean	median	mean	median	mean	median
1	Palmdale to Fairbanks	–*	–	1.4×10^6	1.3×10^6	–	–	17.0	17.9	10.1	9.4	1.78	1.81
2	Fairbanks to Thule	–	–	4.9×10^5	4.7×10^5	–	–	4.7	4.5	2.7	2.9	1.82	1.69
3	Thule to Fairbanks	–	–	9.1×10^5	8.7×10^5	–	–	6.3	5.2	3.3	2.8	1.87	1.88
4	Fairbanks to Iqaluit	1.9×10^5	1.6×10^5	4.9×10^5	4.3×10^5	1.29	0.36	3.2	2.9	2.0	2.1	1.81	1.69
5	Iqaluit to Fairbanks	6.5×10^5	5.2×10^5	6.0×10^5	5.1×10^5	1.81	1.02	–	–	2.8	2.5	–	–
6	Fairbanks local	4.6×10^5	4.6×10^5	5.8×10^5	5.3×10^5	3.78	0.81	–	–	3.2	3.3	–	–
7	Fairbanks local	6.4×10^5	6.1×10^5	7.2×10^5	6.8×10^5	1.24	0.85	6.3	5.9	4.3	4.0	1.44	1.45
8	Fairbanks local	3.7×10^5	3.0×10^5	4.7×10^5	4.2×10^5	1.46	0.73	4.3	4.3	2.4	2.2	1.84	1.74
9	Fairbanks to Palmdale	1.0×10^6	8.0×10^5	1.5×10^6	1.3×10^6	0.72	0.66	12.5	11.9	7.7	7.1	1.67	1.64
	ARCTAS-A (Flt#1–9)	5.2×10^5	4.1×10^5	6.9×10^5	5.6×10^5	1.74	0.72	6.3	5.0	3.8	3.0	1.72	1.65
10	Palmdale local	6.5×10^6	5.9×10^6	8.2×10^6	8.1×10^6	0.77	0.75	26.7	26.5	28.3	27.9	0.97	0.94
11	Palmdale local	7.1×10^6	7.1×10^6	7.5×10^6	7.5×10^6	0.88	0.86	19.6	19.0	28.9	28.5	0.70	0.65
12	Palmdale local	5.3×10^6	4.4×10^6	4.2×10^6	4.1×10^6	1.21	1.12	21.0	20.7	17.1	17.2	1.30	1.20
13	Palmdale local	–	–	5.6×10^6	4.3×10^6	–	–	24.5	21.7	20.0	19.1	1.44	1.25
14	Palmdale to Cold Lake	4.1×10^6	3.5×10^6	3.9×10^6	3.8×10^6	1.04	1.02	24.2	25.4	20.3	20.3	1.85	1.14
	ARCTAS-CARB (Flt#10–14)	5.8×10^6	4.8×10^5	5.9×10^6	4.9×10^6	1.00	0.92	22.9	21.7	22.5	21.3	1.22	1.05
15	Cold Lake local	2.5×10^6	1.6×10^6	2.2×10^6	2.1×10^6	2.15	0.75	15.0	11.5	12.5	9.9	1.45	1.19
16	Cold Lake local	9.7×10^6	6.6×10^5	1.2×10^6	9.4×10^5	0.93	0.75	21.6	23.6	14.5	13.7	1.58	1.41
17	Cold Lake local	2.7×10^6	1.9×10^6	2.3×10^6	1.8×10^6	1.16	1.07	25.5	27.1	19.7	20.5	1.36	1.28
18	Cold Lake local	2.2×10^6	1.1×10^6	1.8×10^6	1.1×10^6	1.27	0.92	14.6	10.7	11.8	8.3	1.06	1.13
19	Cold Lake to Thule	5.6×10^5	4.6×10^5	9.8×10^5	8.4×10^5	0.63	0.55	3.4	3.2	2.6	2.2	1.33	1.35
20	Thule local	1.3×10^6	1.3×10^6	2.3×10^6	2.2×10^6	0.61	0.58	6.3	4.9	10.8	11.3	0.57	0.46
21	Thule to Cold Lake	1.1×10^6	1.0×10^6	2.3×10^6	2.2×10^6	0.51	0.48	13.7	14.0	9.7	9.5	1.49	1.44
22	Cold Lake to Palmdale	2.1×10^6	1.5×10^6	5.1×10^6	3.5×10^6	0.41	0.40	38.8	42.7	34.1	35.0	1.23	1.12
	ARCTAS-B (Flt#14–22)	1.7×10^6	1.1×10^6	1.9×10^6	1.7×10^6	1.10	0.66	16.4	14.7	12.8	11.0	1.33	1.28
	Entire Campaign	2.4×10^6	1.0×10^6	2.6×10^6	1.6×10^6	1.28	0.74	17.1	14.5	15.1	11.4	1.40	1.29

* "–" means no CIMS data available for that flight.

AMTD
5, 2529–2565, 2012

Fig. 1. Pictures showing the setup of the LIF and CIMS instruments for OH and HO_2 measurements on the NASA DC-8 aircraft during ARCTAS 2008.

AMTD
5, 2529–2565, 2012

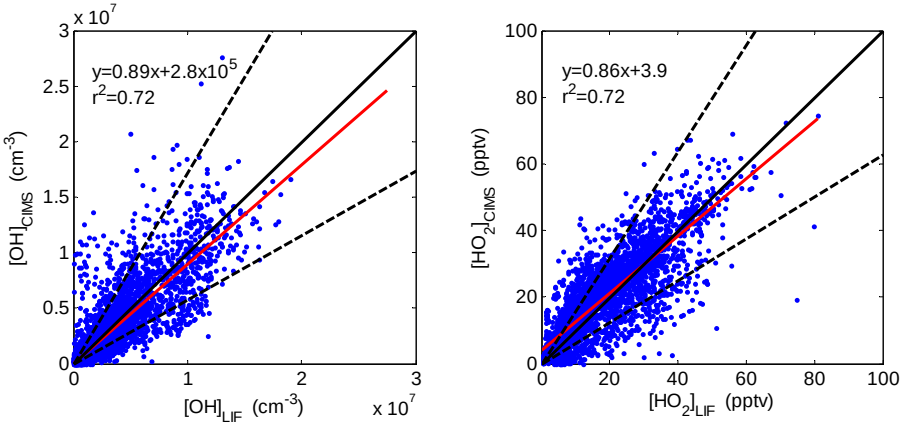

Fig. 2. Scatter plots of CIMS [OH] vs. LIF [OH] (left) and CIMS [HO_2] vs. LIF [HO_2] (right). The red lines illustrate the linear regression and the black solid lines represent 1:1 ratio. The dashed lines indicate the combined measurement uncertainties: ±72 % (2σ) for OH and ±59 % (2σ) for HO_2.

AMTD
5, 2529–2565, 2012

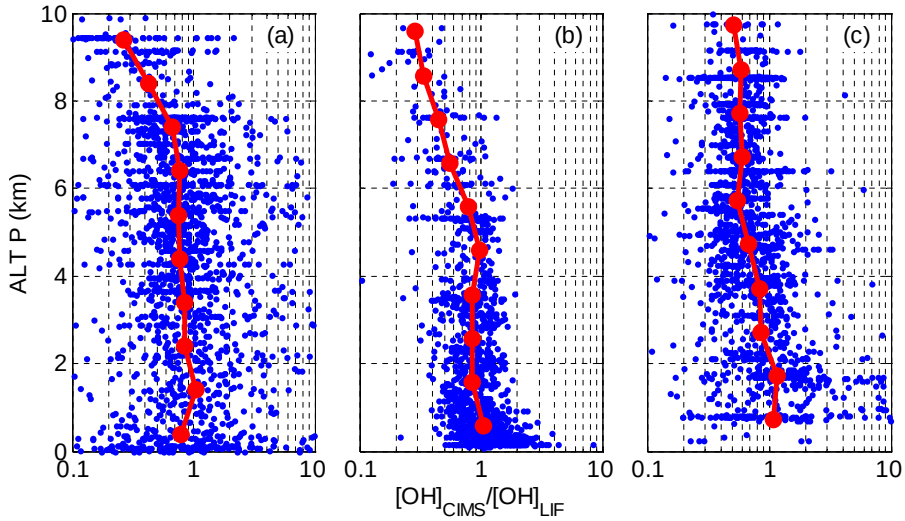

Fig. 3. Observed CIMS-to-LIF OH ratio as a function of altitude during ARCTAS-A **(a)**, ARCTAS-CARB **(b)**, and ARCTAS-B **(c)**. Individual points represent 1-min data and linked circles are the median values of 1-km altitude bins.

AMTD
5, 2529–2565, 2012

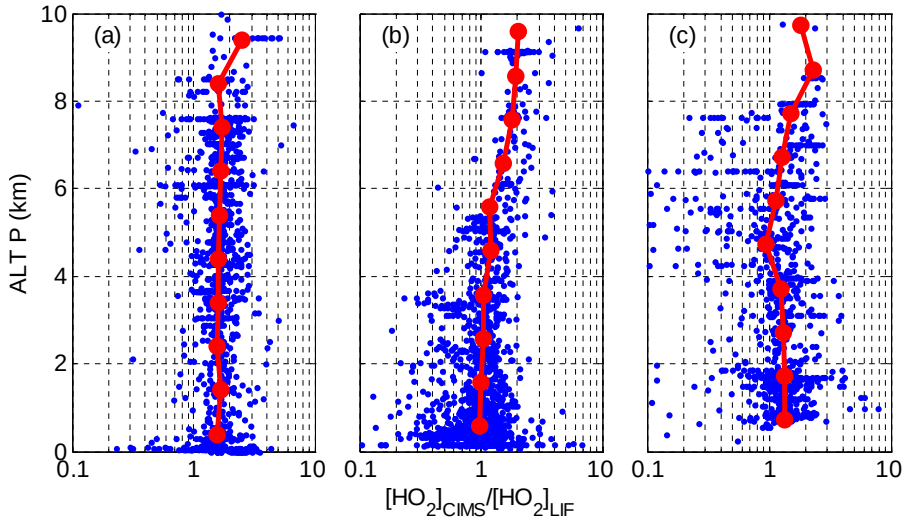

Fig. 4. Observed CIMS-to-LIF HO_2 ratio as a function of altitude during ARCTAS-A **(a)**, ARCTAS-CARB **(b)**, and ARCTAS-B **(c)**. Individual points represent 1-min data and linked circles are the median values of 1-km altitude bins.

AMTD
5, 2529–2565, 2012

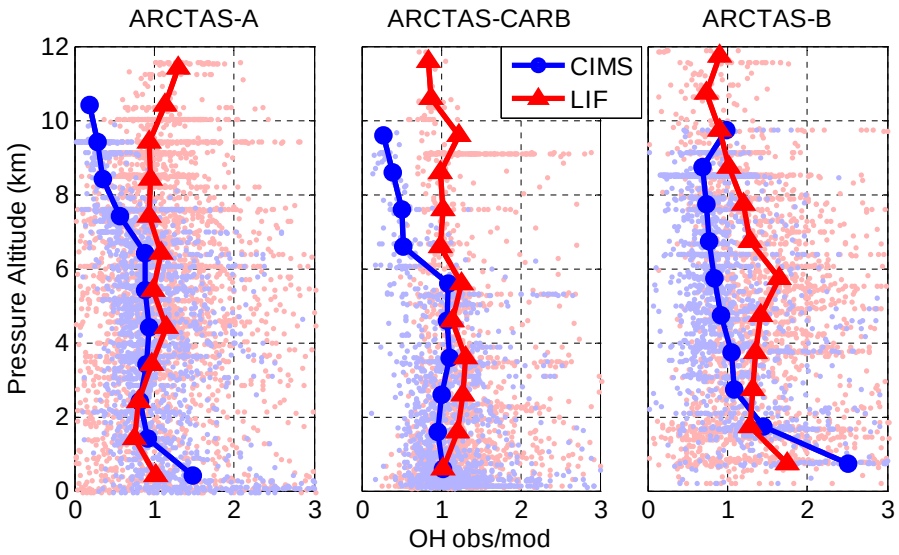

Fig. 5. Measured-to-modeled OH as a function of altitude during ARCTAS-A (left), CARB (middle) and ARCTAS-B (right) phases of ARCTAS. Comparisons of the box model with CIMS (blue) and LIF (red) are shown as 1-min measurements (small dots) and as 1-km median values (linked symbols).

AMTD
5, 2529–2565, 2012

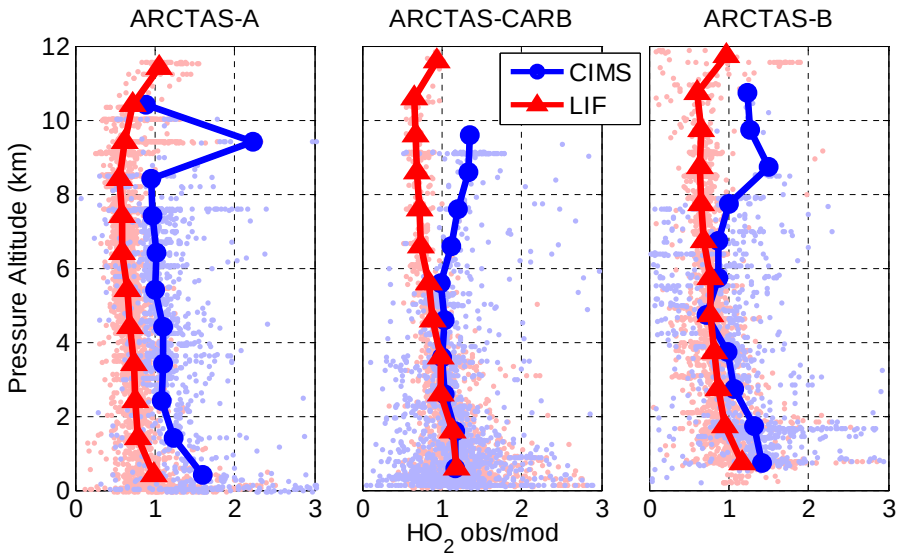

Fig. 6. Measured-to-modeled HO_2 as a function of altitude during ARCTAS-A (left), ARCTAS-CARB (middle) and ARCTAS-B (right). Comparisons of the box model with CIMS (blue) and LIF (red) are shown as 1-min measurements (small dots) and as median values in 1-km bins (linked symbols).

AMTD
5, 2529–2565, 2012

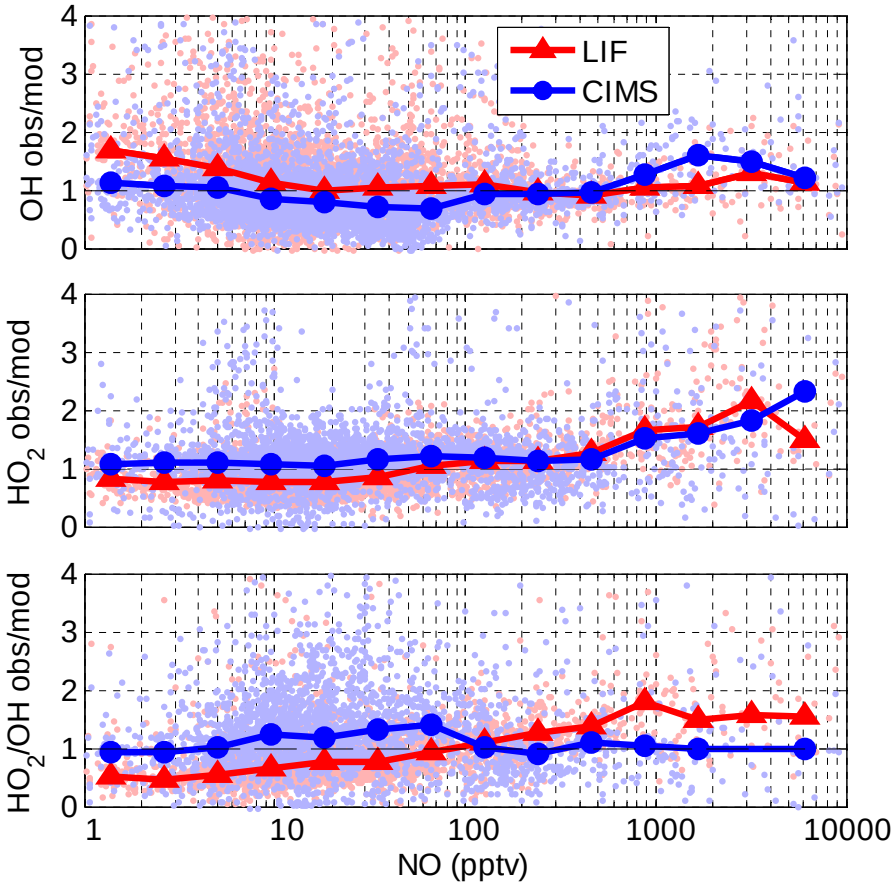

Fig. 7. NO dependence of observed-to-modeled OH (top) and HO_2 (middle) and HO_2/OH (bottom) ratios for LIF (red) and CMS (blue) measurements during ARCTAS. Individual points are 1-min averaged data and linked symbols indicate median values in NO mixing ratio bins.

AMTD
5, 2529–2565, 2012

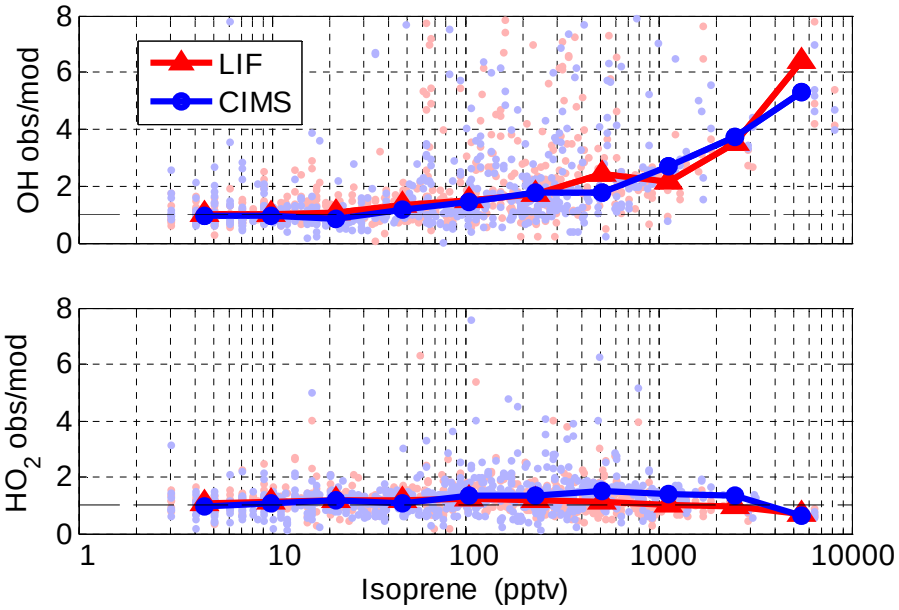

Fig. 8. Observed-to-modeled OH (top) and HO_2 (bottom) ratios for LIF (red) and CIMS (blue) measurements as a function of isoprene. Individual points are 1-min averaged data and linked symbols indicate median values in isoprene mixing ratio bins.

AMTD
5, 2529–2565, 2012